AD-A130 988 FUNDAMENTAL STUDY OF NUCLEAR PUMPED LASER PLASMAS(U) 1/1
MIAMI UNIV OXFORD OH DEPT OF PHYSICS L W DOWNES ET AL.
23 DEC 80 DASG60-78-C-0089

UNCLASSIFIED F/G 20/5 NL

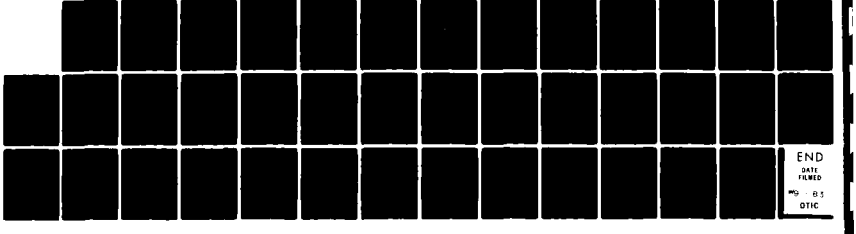

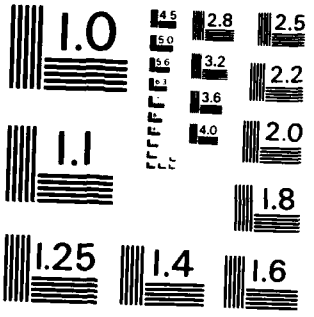

Special Report

to

The United States Army

BMDATC

Contract

DASG 60-78-C-0089

on

Fundamental Study of Nuclear Pumped Laser Plasmas

December 23, 1980

by

L. W. Downes

S. D. Marcum

R. A. Tilton

W. E. Wells

Submitted by

W. E. Wells
Associate Professor
Department of Physics
Miami University
Oxford, Ohio 45056

I. Introduction

Although there have been many activities during the preceding report periods, this interim report will restrict itself to the theoretical prediction of a new laser amplifier process and experimental evidence for the existence of the process. This special report is being generated because this new laser process may have significant impact on nuclear pumped lasers, as well as high power (and high energy) laser systems in general.

II. A Laser Amplifier Based on Radiative Collisions

In 1972, Gudzenko and Yakovlenko[1] described a process involving, effectively, a three-body collision between atomic or molecular species X and Y, and a photon $\hbar\omega$.

Figure 1 shows an energy level diagram for atoms X and Y. The reaction predicted by the Russians is,

$$Y(2) + X(1) + \hbar\omega \rightarrow Y(1) + X(2). \tag{1}$$

The photon having an energy $\hbar\omega$ creates a resonant three-body collision. The rate of production of state X(2) is

$$\frac{d[X(2)]}{dt} = k\rho\,[Y(2)]\,[X(1)], \tag{2}$$

where [] indicates concentrations, ρ is the photon flux field and k is a rate coefficient for this new radiative collision. If we cast this in terms of a normal binary collision, then

$$k\rho = \langle \sigma v \rangle \ , \tag{3}$$

where σ is the cross section and v is the relative velocity, thus (2) becomes

$$\frac{d[X(2)]}{dt} = \langle \sigma v \rangle\,[Y(2)]\,[X(1)]. \tag{4}$$

Alternatively, if we cast this in terms of photon absorption, then

$$k[Y(2)] = B_{12} \ , \tag{5}$$

where B_{12} is the Einstein B coefficient and we may write (2) as

$$\frac{d[X(2)]}{dt} = B_{12}\,\rho\,[X(1)] \ . \tag{6}$$

When cast in the form of a collision, as in (3)and(4), the cross-section, σ , becomes a function of ρ, the photon flux field. When written in the form of a radiative absorption, as in (5) and (6), the Einstein stimulated

RADIATIVE COLLISIONS
(ABSORPTION)

$$Y(2) + X(1) + \hbar\omega \rightarrow X(2) + Y(1)$$

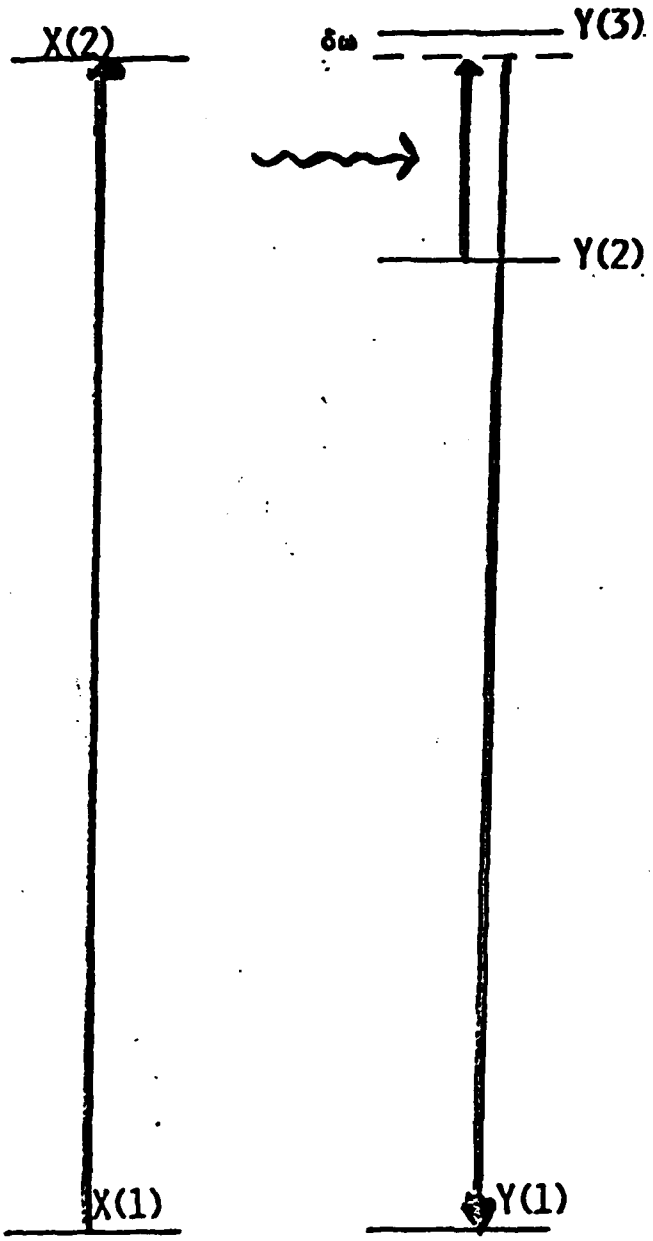

GUDZENKO AND YAKOVLENKO, 1972

Figure 1. Radiative collision, absorption.

absorption coefficient B_{12} becomes a function of the density, [Y(2)], and the photon, $\hbar\omega$, does not have the energy of the difference between X(2) and X(1). A third method of describing these collisions would be the absorption of a photon by a quasi-molecule Y(2)X(1). This model is very useful and will be discussed later.

Harris[3] has used the collsional model to describe his observations of many such collisions he and his colleagues have observed. Figure 2 taken from Harris[3] indicates some of the experimental observations made by his group. An examination of this list indicates some very large cross-sections for a wide variety of collisions induced by intense photon flux fields. The largest cross-section reported elsewhere is $8 \times 10^{-13} cm^2$.

Such a cross section is three orders of magnitude above gas kinetic type collisions. It is large enough to control the energy pathways in a plasma. Harris[3] and others[4] have used this fact to propose <u>population mechanisms</u> for lasers.

Our proposal for a new stimulated-emission process (not only a new laser) is based on the inverse process to (1). This process was considered briefly in Reference 1,

$$\hbar\omega + X(2) + Y(1) \rightarrow X(1) + Y(2) + 2\hbar\omega \ . \tag{7}$$

This is demonstrated in the energy level diagram in Figure 3. For reaction (7), the colliding atoms are stimulated to emit a photon, where in reaction (1) the colliding atoms are stimulated to absorb a photon. The cross-section for the two reactions, (1) and (7), are the same; thus the rate of production will be the difference between the two processes:

$$\frac{d[X(2)]}{dt} = k\rho \{[Y(2)][X(1)] - [X(2)][Y(1)]\} \tag{8}$$

Since the negative term produces photons, the photon production rate is

$$- \frac{d[X(2)]}{dt}(\hbar\omega) = \frac{d\rho}{dz} \tag{9}$$

If the statistical weights are also considered, then the gain in photon

Process	Comments	Collision Cross Section (Laser Power Density)	Reference
$Sr(5s5p\ ^1P_1^o) + Ca(4s^2\ ^1S_0) + h\nu(6409\ \text{Å}) \rightarrow Sr(5s^2\ ^1S_0) + Ca(4d\ ^1D)$	Recall		6
$Sr(5s5p\ ^1P_1^o) + Ca(4s^2\ ^1S_0) + h\nu(4977\ \text{Å}) \rightarrow Sr(5s^2\ ^1S_0) + Ca(4p^2\ ^1S_0)$	Dipole-Dipole Weak Field	$9 \times 10^{-18}\ cm^2$ ($5 \times 10^5\ W/cm^2$)	4
$Sr(5s5p\ ^1P_1^o) + Ca(4s^2\ ^1S_0) + h\nu(4711\ \text{Å}) \rightarrow Sr(5s^2\ ^1S_0) + Ca(5d\ ^1D)$	Dipole-Dipole Weak Field		4
$Sr(5s5p\ ^1P_1^o) + Ca(4s^2\ ^1S_0) + h\nu(4977\ \text{Å}) \rightarrow Sr(5s^2\ ^1S_0) + Ca(4p^2\ ^1S_0)$	Dipole-Dipole Strong Field	$4 \times 10^{-13}\ cm^2$ ($3 \times 10^{10}\ W/cm^2$)	5
$Ca(4s4p\ ^1P_1^o) + Sr(5s^2\ ^1S_0) + h\nu(6217\ \text{Å}) \rightarrow Ca(4s^2\ ^1S_0) + Sr(5s6d\ ^1D_2)$	Dipole-Dipole Strong Field	$10^{-14}\ cm^2$ ($3 \times 10^9\ W/cm^2$)	5
$Sr(5s5p\ ^1P_1^o) + Ca(4s^2\ ^1S_0) + h\nu(5307\ \text{Å}) \rightarrow Sr(5s^2\ ^1S_0) + Ca(3d4p\ ^1F_3^o)$	Dipole-Quadrupole	$3 \times 10^{-14}\ cm^2$ ($7 \times 10^9\ W/cm^2$)	2
$Ca^+(4s\ ^2S_{1/2}) + Sr(5s^2\ ^1S_0) + h\nu(4715\ \text{Å}) \rightarrow Ca(4s^2\ ^1S_0) + Sr^+(5p\ ^2P_{3/2}^o)$	Charge Transfer to an Excited Ionic State	$5 \times 10^{-15}\ cm^2$ ($1.5 \times 10^9\ W/cm^2$)	1
$Ba(6p\ ^1P_1^o) + Ba(5d\ ^1D_2) \rightarrow 2Ba(6s^2\ ^1S_0) + h\nu(3394\ \text{Å})$	Radiative Fluorescence	$\sigma_{spontaneous} = 2.6 \times 10^{-20}\ cm^2$	8
$Ba(6s^2\ ^1S_0) + Ba(6s^2\ ^1S_0) + h\nu(3394\ \text{Å}) \rightarrow Ba(6p\ ^1P_1^o) + Ba(5d\ ^1D_2)$	Pair Absorption		10
$Ba(6s^2\ ^1S_0) + Tl(6p\ ^2P_{1/2}^o) + h\nu(3867\ \text{Å}) \rightarrow Ba(6p\ ^1P_1^o) + Tl(6p\ ^2P_{3/2}^o)$	Pair Absorption		10

Figure 2. Radiative collisional cross sections (after Harris).

RADIATIVE COLLISIONS (EMISSION)

$$X(2) + Y(1) + \hbar\omega \rightarrow X(1) + Y(2) + 2\hbar\omega$$

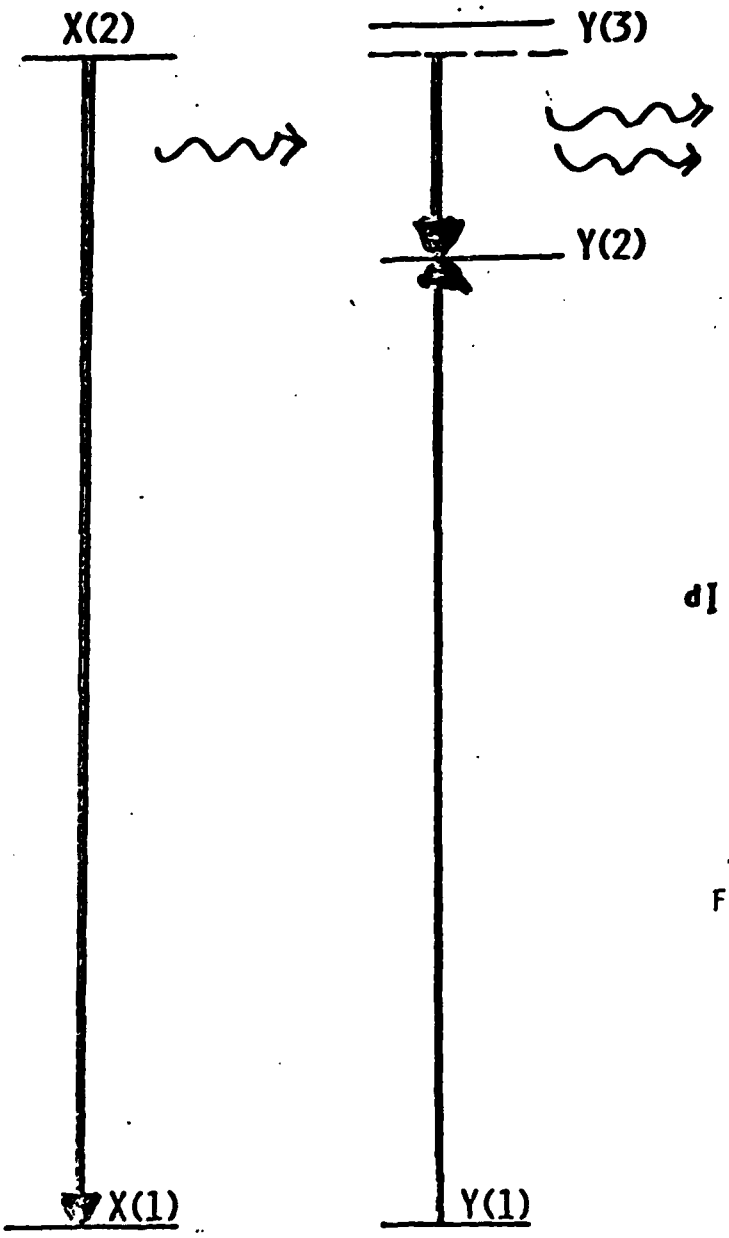

$$dI = \hbar\omega\langle\sigma v\rangle \left(G_1[X(2)][Y(1)] - (G_2[X(1)][Y(2)]\right) dZ$$

Figure 3. Radiative collision, emission.

flux can be expressed as

$$\text{Gain} = \frac{d\rho}{\rho dz} = \hbar\omega k\{[g_{X(2)}\, g_{Y(1)}\, [X(2)][Y(1)] - g_{Y(2)}\, g_{X(1)}[Y(2)][X(1)]\} \quad (10)$$

Note that the gain of such a system depends on an inversion of the products of the densities. This provides new ways to produce inversions, for the energy storage can be in one atom for the upper laser levels and the lower levels can be deactivated in its collision partner. Harris'[3] data indicates, at high photon flux fields, the large cross-section would make the radiative collision the chief energy pathway, forcing the photon production efficiency to the quantum efficiency. At lower photon flux fields, the energy is channeled through other processes and the efficiency would be expected to be very low. An example of this is shown next for a system of helium and nitrogen.[2] Although better systems do exist, the abundance of atomic and molecular data for helium and nitrogen makes this example useful.

Figure 4 shows the energy level diagram for helium and nitrogen. In this system, we can make the correspondence between

$$X(1) \rightarrow He(1^1s)$$
$$X(2) \rightarrow He(2^3s)$$
$$Y(1) \rightarrow N_2(X)$$
$$Y(2) \rightarrow N_2^*(X, v = 3)$$
$$Y(3) \rightarrow N_2^*(B, v = 4).$$

Note that in the nitrogen the * denotes excitation to a Rydberg state near the ionization limit. The reaction of interest now becomes

$$He(2^3S) + N_2(X) + \hbar\omega \rightarrow He(1^1S) + N_2^*(X, v=3) + 2\hbar\omega \; . \quad (11)$$

Because the Rydberg electron is near the ionization limit (in or near the Saha region), the Y(3), N_2^* (B, v = 4), state is nearly resonant with $He(2^3S)$ and the induced transition can be considered in the same manner as the equivalent ionic state. Figure 5 gives the wavelengths and Einstein coefficients for the $N_2^+(B,v') \rightarrow N_2^+(X,v'')$ transition. This figure indicates that the 3538Å wavelength transition is probably best for reaction (11).

Harris[3] has derived an expression for the cross-section for a dipole-

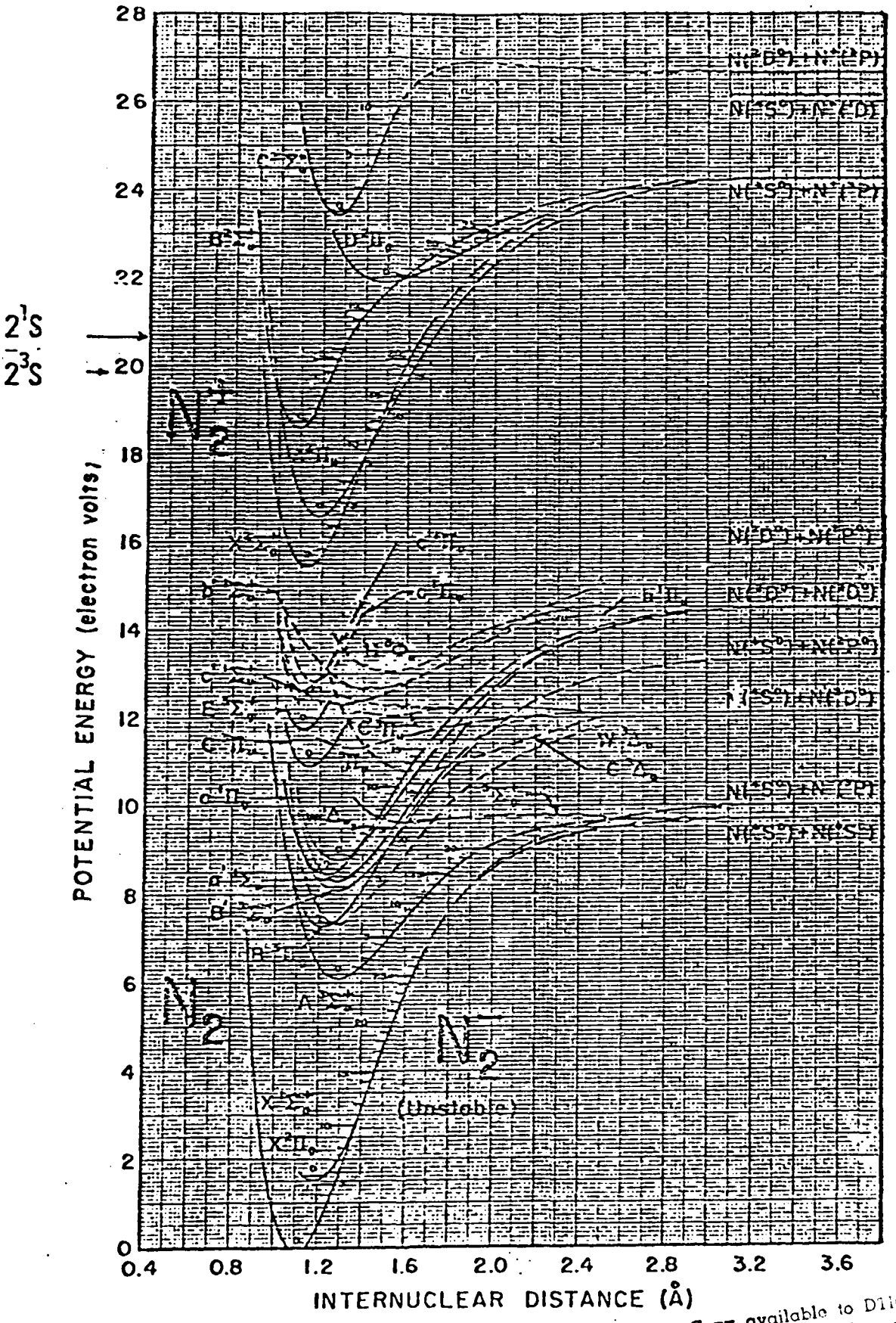

Figure 4. Nitrogen potential energy curve.

Figure 5.

N_2^+(B X) Potential Curves, Transition Wavelengths and A Coefficients

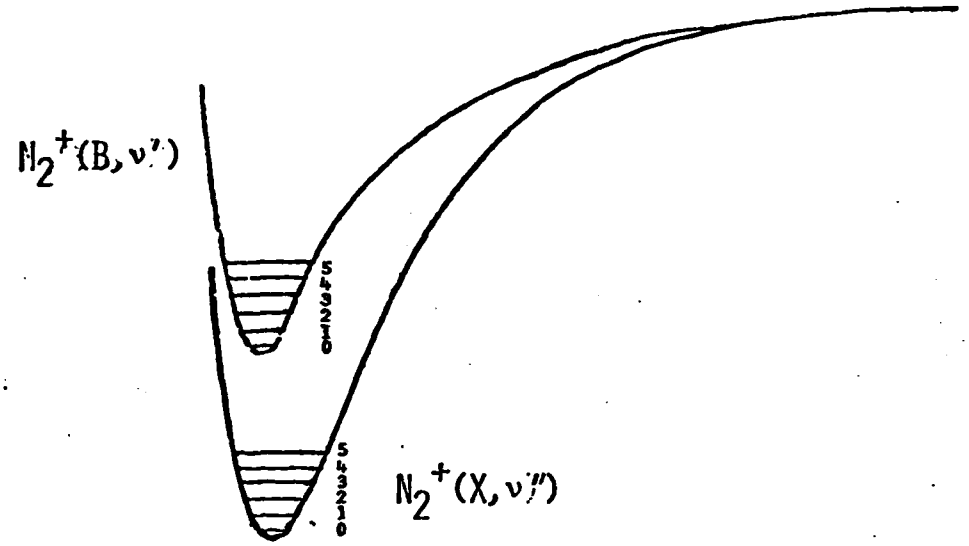

v' \ v''	0	1	2	3	4	5
0	9.64 3914.4	3.48 4278.	.775 4709.	.136 5228.	.206 5864.	.283
1	4.87 3582.	3.08 3884.3	3.87 4236.	1.53 4652.	.392 5149.	.078 5653.
2	.757 3308.	6.36 3564.	.574 3857.9	3.03 4199.	1.94 4560.	.68 5077.
3	.028 3078.	1.64 3299.	6.24 3549.	.003 3835.4	1.98 4167.	2.00 4554.
4		.062 3076.	2.35 3293.	5.55 3538.	.154 3818.1	1.14 4140.
5			.072	2.78 3291.	4.83 3532.	.431 3806.8

Einstein coefficients (in units of 10^{-6}s) and Wavelengths (in Angstroms) for the 1st Negative System of Nitrogen

quadrupole radiative collision for strong and weak photon flux field limits. In this expression, shown in Figure 6, the dipole matrix element, μ_{21} , is determined by the energy[5] and the Franck-Condon factor[6], μ_{32} is estimated from the table in Figure 5, and q_{12} is estimated from the equivalent singlet lifetime considering electron exchange during the collision.

Since the Rydberg state is effectively in the Saha continuum, the detuning energy, $\delta\omega$, is taken to be a collection of the linewidths of the three states and the bandwidth of the incoming photon flux field. The value is estimated to be 2 cm^{-1}. Figure 7 shows the cross-section as a function of photon flux field, for both the strong and weak field cases. Using that cross-section, a model has been developed for helium-nitrogen. The rate equations for this are given in Figure 8.

The model has been solved in the steady state for power depositions between 20W/cm^3 and 20MW/cm^3 in one atmosphere of helium and various percentages of nitrogen. The data presented here is for 1% nitrogen.

The gain of the system is calculated from equation (10). It should be emphasized that the N_2^* (X,v=3) is an auto-ionizing state[7] which has a lifetime of about 10^{-10}sec. This makes the product density $[He\ 1^1_S][N_2^*(X,v=3)]$ negligible because the lower levels self-destruct. The gain for the system is shown in Figure 9. The reason for the decrease in gain at higher photon fluxes is due to the high destruction rate for helium metastables. The metastable density as a function of photon flux is shown in Figure 10. The efficiency is shown in Figure 11 and saturates near the quantum efficiency of about 15%. At low photon flux fields, the efficiency becomes very poor (so poor that an oscillator function is probably out of the question). But at high photon fluxes, the efficiency is quite acceptable for laser amplification (see conclusions).

$$He(2^3S) + N_2 + \hbar\omega \rightarrow N_2^*(x,v) + He + 2\hbar\omega$$

$$N_2^*(x,v) \longrightarrow N_2^+(x,v-1) + e$$

$$\sigma_{weak} = \left(\frac{\pi^3}{2\hbar^2 \bar{v}^2} \right) \left(\frac{3\mu_{21}^{N_2^*} q_{12}^{He}}{2\rho_0^2} \right)^2 \left(\frac{\mu_{23}^{N_2^*} E}{2\hbar\Delta\omega} \right)^2$$

$$\sigma_{strong} = \left[\left(\frac{\pi}{\hbar\bar{v}} \right) \left(\frac{3\mu_{21}^{N_2^*} q_{12}^{He}}{2} \right) \left(\frac{\mu_{23}^{N_2^*} E}{2\hbar\Delta\omega} \right) \right]^{2/3} \pi$$

μ_{21} = dipole matrix element $N_2 \rightarrow N_2^*(B,v)$

μ_{23} = dipole matrix element $N_2^*(B,v) \rightarrow N_2^*(X,v)$

q_{12} = quadrupole matrix element $He(2^3S) \rightarrow He$

ρ_0 = Weisskopf radius

$\Delta\omega$ = detuning energy

$\bar{v}$ = plasma velocity

E = photon field

Figure 6. Strong and weak field cross sections.

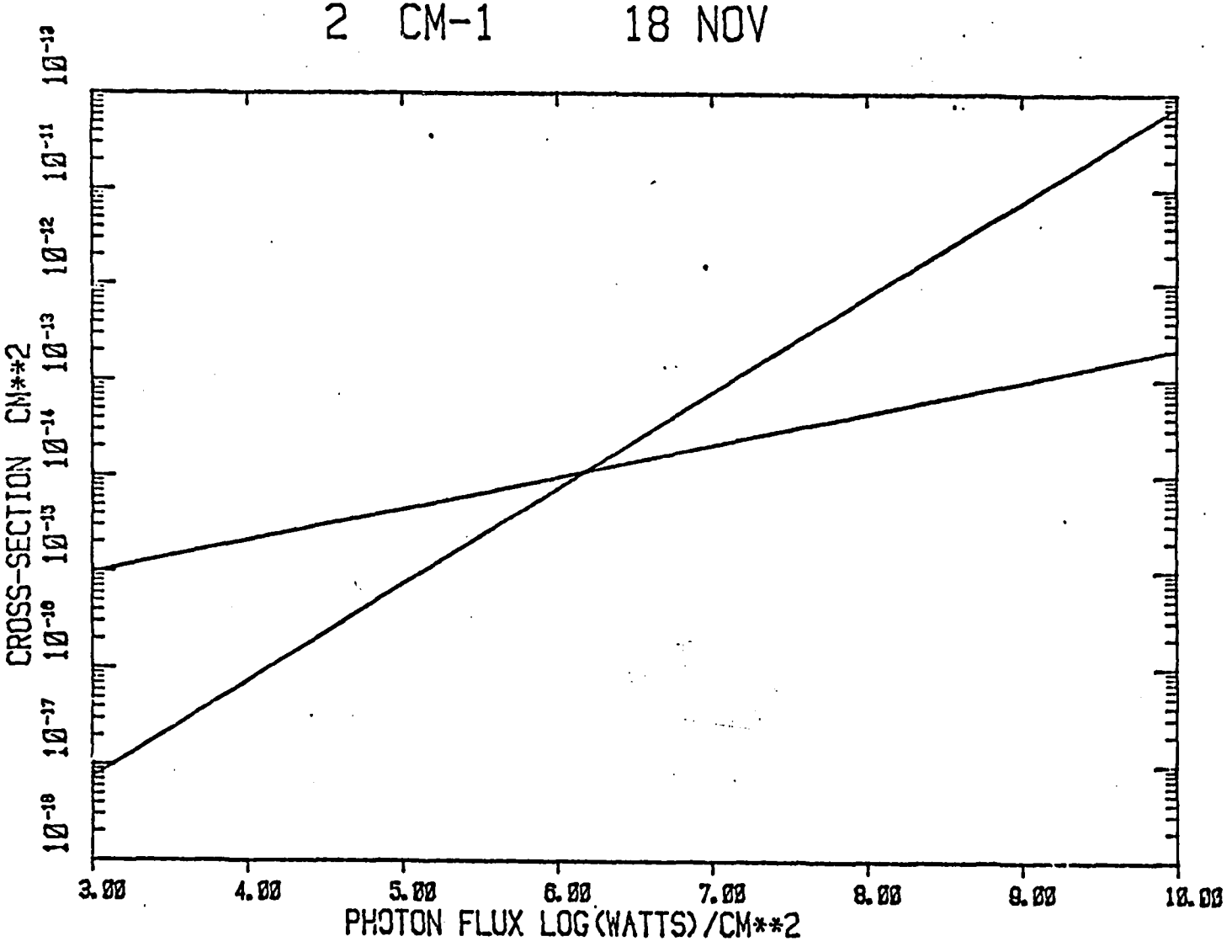

Figure 7. Radiative collisional cross section from model calculation in He-N_2 system.

RATE EQUATIONS FOR HE-N_2 SYSTEM

1. $$\frac{d[He^+]}{dt} = S + \frac{\beta}{2}[He(2^3S)]^2 - k_1[N_2][He^+] - k_2 p_{He}^2 [He^+]$$

S - ENERGY DEPOSITED/SEC/CM^3 / W VALUE (ENERGY EXPENDED FOR 1 ION)

$\beta \rightarrow He(2^3S) + He(2^3S) \rightarrow He^+ + He + e$ METASTABLE-METASTABLE IONIZATION

$k_1 \rightarrow N_2 + He^+ \rightarrow N_2^+ + He$ CHARGE EXCHANGE

$k_2 \rightarrow 2\ He + He^+ \rightarrow He_2^+ + He$ THREE-BODY CONVERSION

2. $$\frac{d[He_2^+]}{dt} = k_2 p_{He}^2 [He^+] - .7\alpha[He_2^+][e] - k_{30}[N_2][He_2^+] - k_{31}[N_2][He_2^+][He]$$

$k_2 \rightarrow 2\ He + He^+ \rightarrow He_2^+ + He$ THREE-BODY CONVERSION

$\alpha \rightarrow He_2^+ + e + X \rightarrow$ COLLISIONAL RADIATIVE RECOMBINATION

$k_{30} \rightarrow N_2 + He_2^+ \rightarrow N_2^+ + 2\ He$ 2-BODY CHARGE TRANSFER

$k_{31} \rightarrow N_2 + He_2^+ \rightarrow N_2^+ + 2\ He + He$ 3-BODY CHARGE TRANSFER

Figure 8. Rate equations for He-N_2 system. (Other rate equations shown next two pages).

3. $$\frac{d[He(2^3S)]}{dt} = S_m + 0.7\,\alpha[He_2^+][e] - \beta[He(2^3S)]^2 - \langle\sigma' v\rangle[N_2][He(2^3S)]$$
$$- A'[N_2][He(2^3S)] - 0.6p_{He}^2[He(2^3S)] - k_{40}[N_2][He(2^3S)]$$
$$- k_{41}[N_2][He(2^3S)][He] - k_5[He(2^3S)][e]$$

$S_m \Rightarrow S/0.56$

$\alpha \Rightarrow He_2^+ + e \rightarrow CRR \rightarrow He(2^3S)$ (70%)

$\beta \Rightarrow He(2^3S) + He(2^3S) \rightarrow He^+ + He + e$ METASTABLE-METASTABLE IONIZATION

$k_{40} \Rightarrow N_2 + He(2^3S) \rightarrow N_2^+ + He + e$ TWO-BODY PENNING IONIZATION

$k_{41} \Rightarrow N_2 + He(2^3S) + He \rightarrow N_2^+ + 2He + e$ THREE-BODY PENNING IONIZATION

$k_5 \Rightarrow He(2^3S) + e \rightarrow He + e$ (20 ev) SUPERELASTIC COLLISION

$\sigma' \Rightarrow \sigma_{weak}\rho$ WEAK FIELD DIPOLE-QUADRUPOLE INTERACTION

$A' \Rightarrow$ EINSTEIN COEFFICIENT SPONTANEOUS PHOTON EMISSION

$0.6p_{He}^2 \Rightarrow He(2^3S) + 2\,He \rightarrow He_2(2^3\Sigma)$ THREE-BODY CONVERSION TO MOLECULAR METASTABLE

Figure 8, continued.

4. $$\frac{d[N_2^+]}{dt} = k_1'[He^+][N_2] + k_{30}[He_2^+][N_2] + k_{31}[He_2^+][N_2][He]$$

$$+ k_{40}[He(2^3S)][N_2] + k_{41}[He(2^3S)][N_2][He]$$

$$+ \langle\sigma' v\rangle[He(2^3S)][N_2] + A'[He(2^3S)][N_2] - \alpha_{N_2}[e][N_2^+]$$

$k_1' \Rightarrow He^+ + N_2 \rightarrow He + N_2^+$ CHARGE EXCHANGE

$k_{30} \Rightarrow He_2^+ + N_2 \rightarrow 2He + N_2^+$ TWO-BODY CHARGE TRANSFER

$k_{31} \Rightarrow He_2^+ + N_2 + He \rightarrow 2He + He + N_2^+$ THREE-BODY CHARGE TRANSFER

$k_{40} \Rightarrow He(2^3S) + N_2 \rightarrow He + N_2^+ + e$ TWO-BODY PENNING IONIZATION

$k_{41} \Rightarrow He(2^3S) + N_2 + He \rightarrow 2He + N_2^+ + e$ THREE-BODY PENNING IONIZATION

$\alpha_{N_2} \Rightarrow N_2^+ + e \rightarrow N_2^*$ DISSOCIATIVE RECOMBINATION

5. $$[e] = [He^+] + [He_2^+] + [N_2^+]$$

Figure 8, continued.

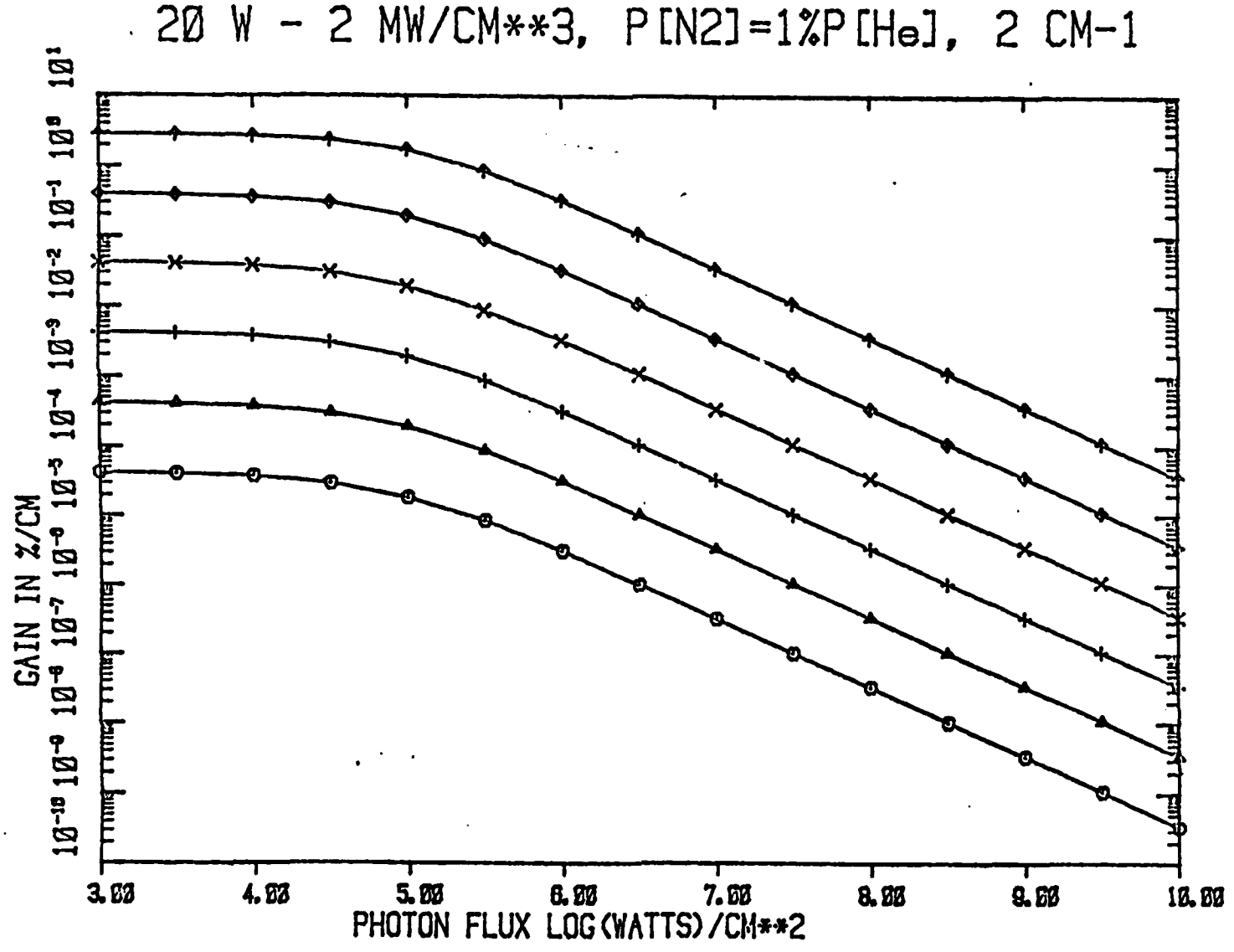

Figure 9. Theoretical gain in the He-N_2 system.

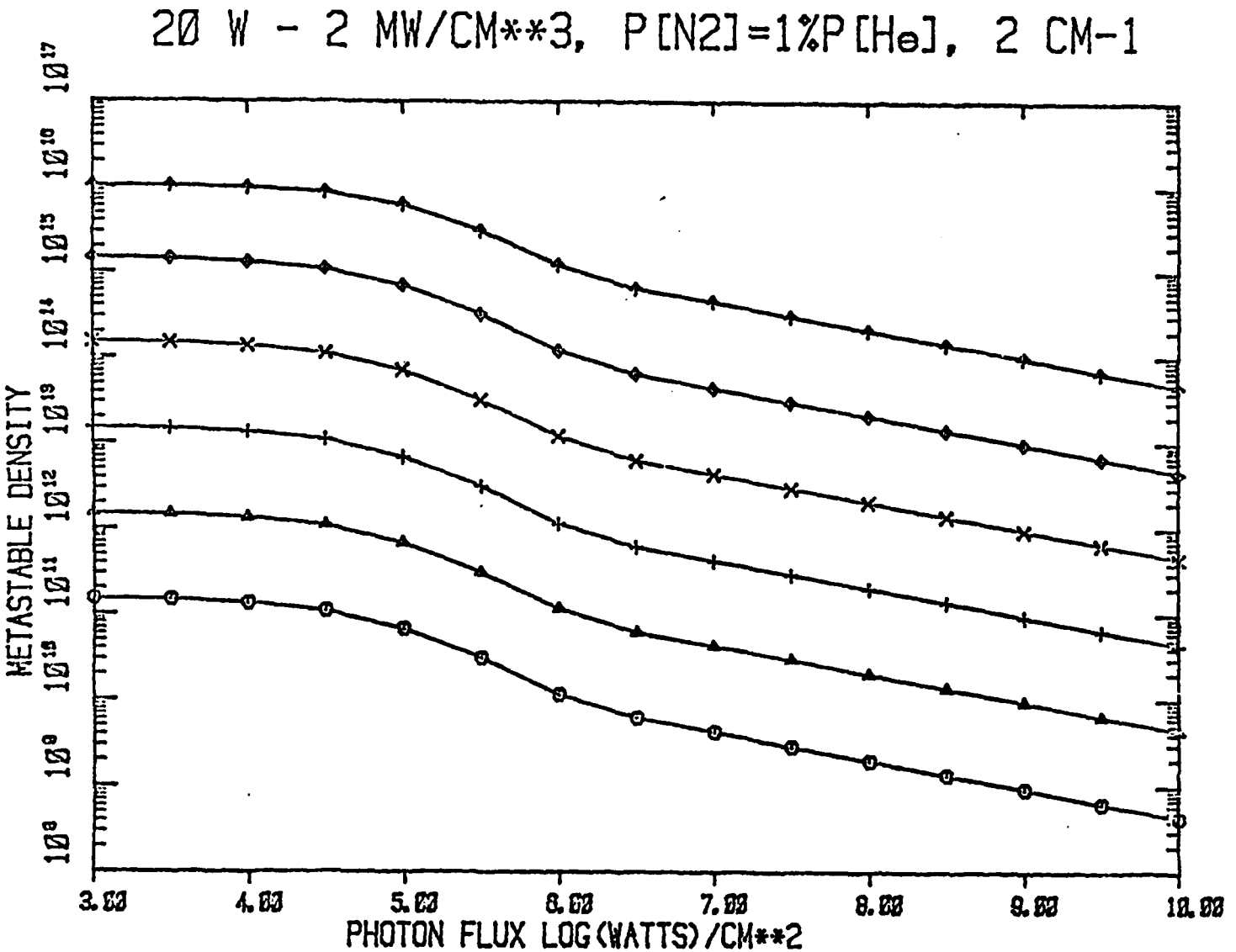

Figure 10. Theoretical helium metastable density for He-N_2 system.

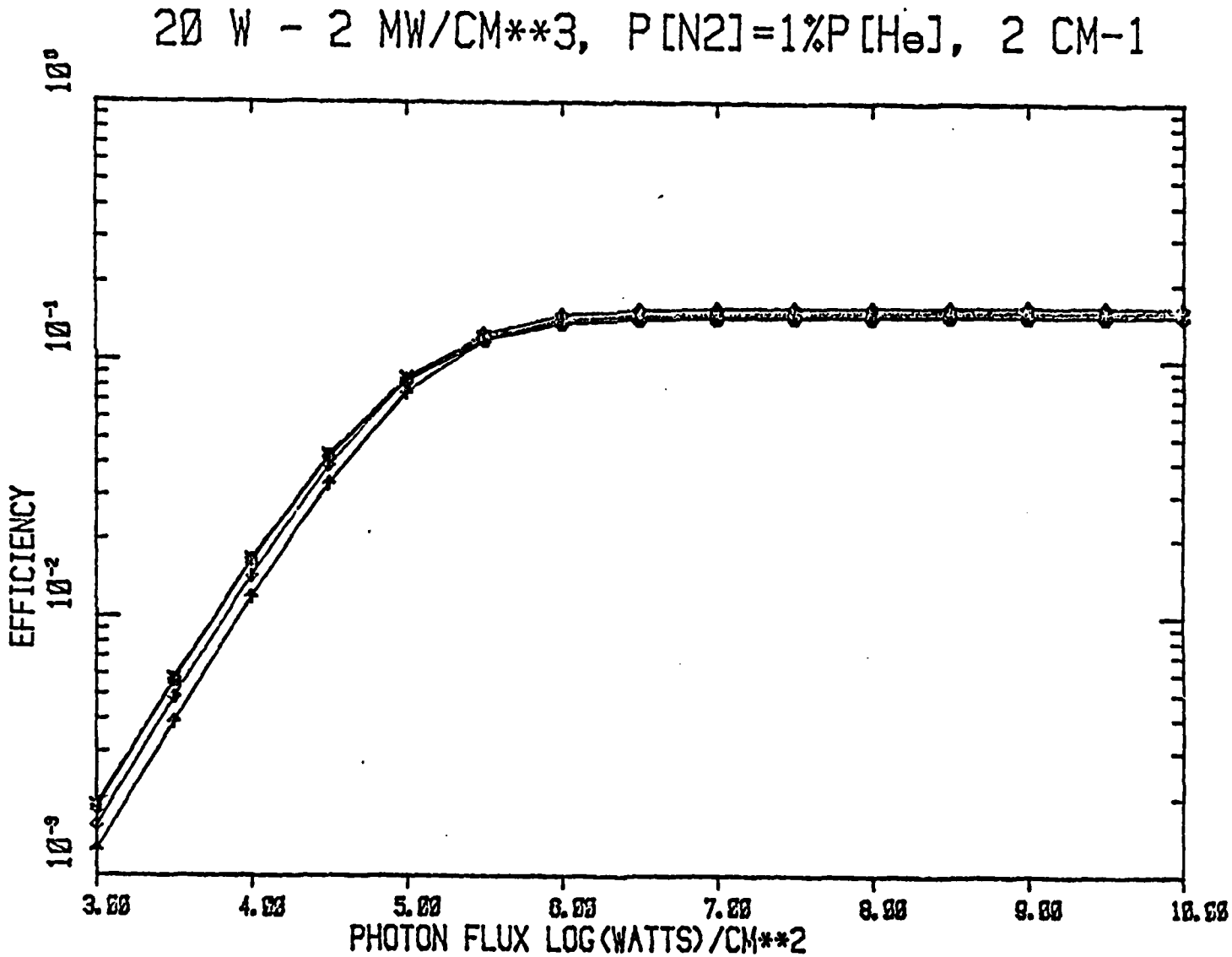

Figure 11. Theoretical efficiencies for the He-N_2 system.

It should be emphasized that although the gain for this system is rather large (see Figure 9), significant energy loss due to superradiance will not be a problem owing to the low efficiency at small photon flux fields. Significant energy extraction will occur only in the direction of the incoming oscillator beam, since the intensity of incoming photon flux determines the cross-section for radiative collisions.

A third method of describing this kind of reaction is the quasi-molecule model. Richardson and Setser[8] have presented the potential energy curves for $He(2^3S)$-N_2 and $He(2^1S)$-$N_2^+(B,\nu=0)$. We have made the assumption that the highly excited Rydberg state is similar to the ionic state, and that the increase in the N_2 vibronic energy affects only the total energy and not the form of the heteronuclear potential energy curves. With these modifications, the Richardson and Setser potential curves appear in Figure 12. The double curve crossing shown here may not be real, but the indication that some curve crossing occurs at large internuclear distances (5 to 7Å) is important. In the quasi-molecule model, the incident photon not only stimulates the production of an identical photon but also enhances the state branching at the curve crossing.

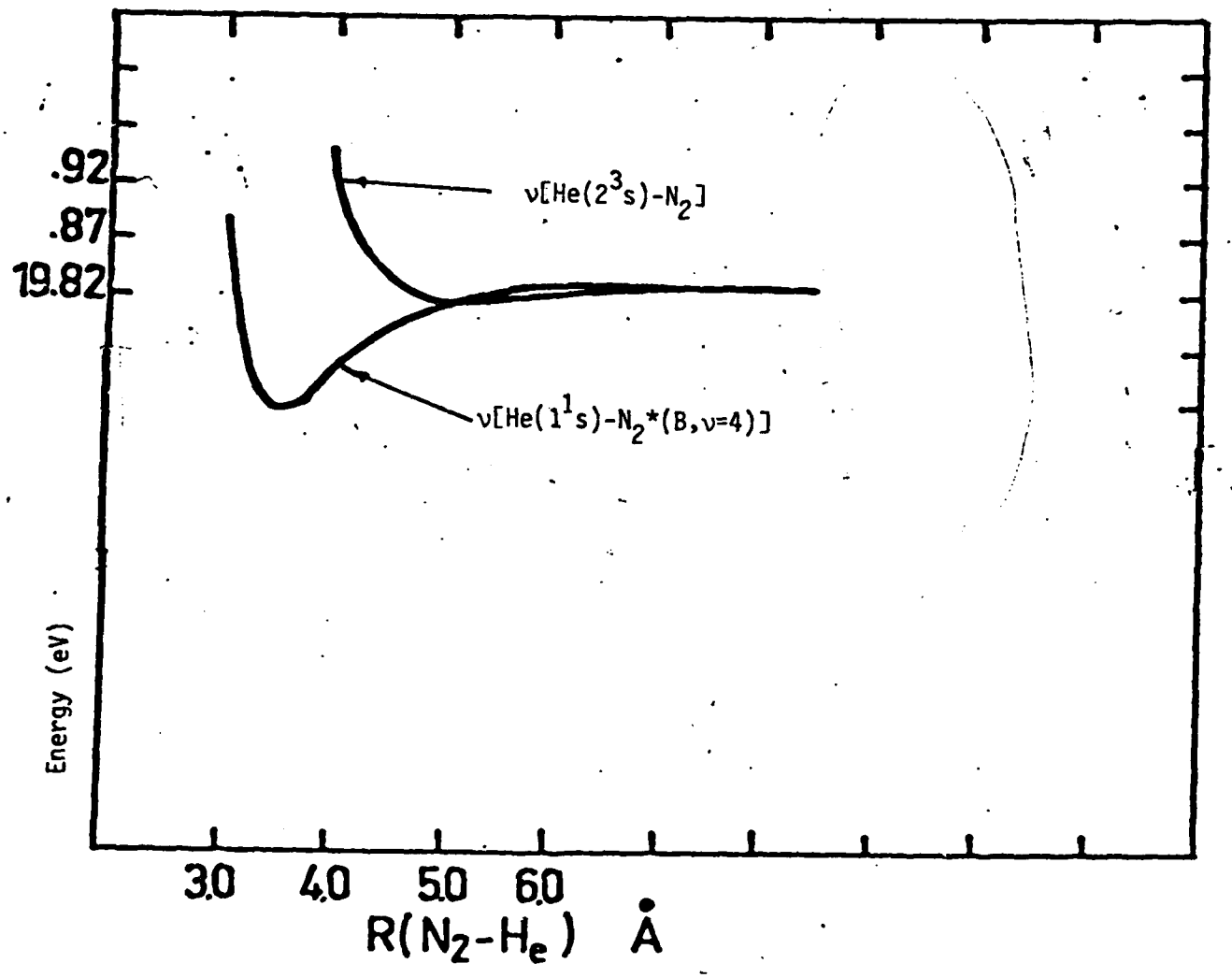

Figure 12. Potential energy curves for $He(2^3s)$-N_2 and $He(1^1s)$-$N_2^*(B,\nu=4)$ after Richardson and Setser (reference 8).

III. Experimental Setup and Data Handling Systems

Figures 13 and 14 depict the experimental apparatus and the data acquisition/reduction systems, respectively, employed in this study. The electron beam device (Maxwell Laboratories, Excitron Model 20-10R) delivers very reproducible pulses of high energy electrons (250kV) at a total transmitted current of 200A transmitted through a 2x10 cm titanium foil ($10A/cm^2$) at a repetition rate of up to 2pps. The plasma cell/gas-handling system obtains base pressures of $5x10^{-8}$ Torr prior to high purity gas fill. The plasma cell is equipped with CaF windows for introduction of the dye laser probe and observation of the plasma. The geometry of the plasma cell is rather different from that of typical systems of this sort due to demands of other experiments. In addition, we are studying basic plasma processes, not demonstrating new lasers. Nevertheless, with a 99%+ He, He-N_2 mixture the energy deposition per unit length is small enough such that the large depth of the cell is not a hinderance at present. A new cell of more conventional geometry is under construction that will allow observation of heavier gases at high pressures (1-5atm.) with consequent higher energy depositions.

The dye laser probe consists of a home-made nitrogen pump laser coupled to a commercially available (Molectron Corp., Model DL-II) tunable dye laser. At present, insufficient N_2-laser power is available to pump both the oscillator and amplifer sections of the dye laser. Without this capability observation of the predicted change in the cross-section for the radiative collisions of interest is difficult. An improved design N_2-pump laser currently under construction and/or negotiations for obtaining either tripled Nd-glass or Nd-YAG pumps will alleviate this situation.

The data acquisition/reduction systems include a 1/2-meter monochromator (Jarrel-Ash, Model 82-000) with output into a UV-peaked

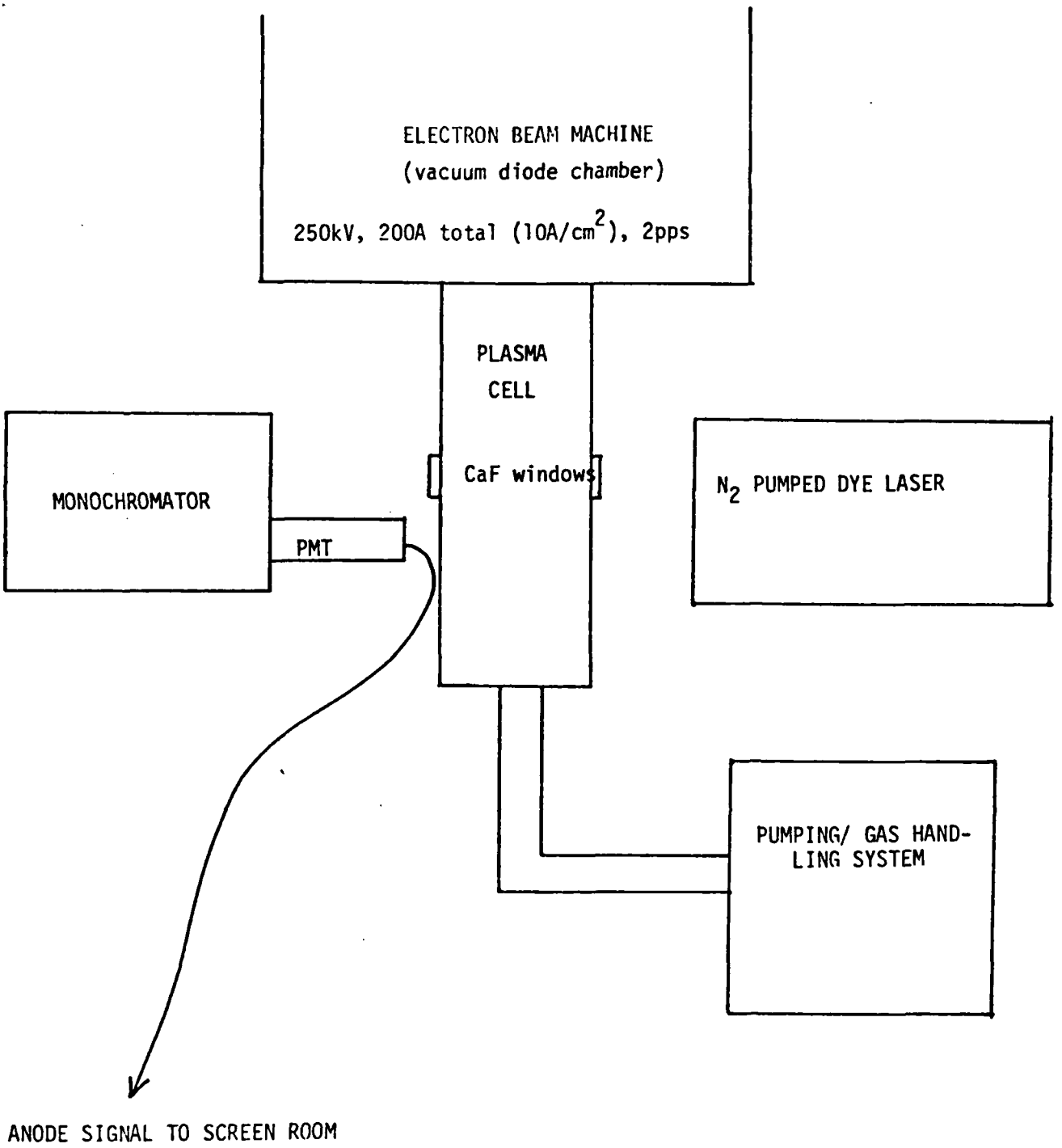

FIGURE 13 EXPERIMENTAL APPARATUS

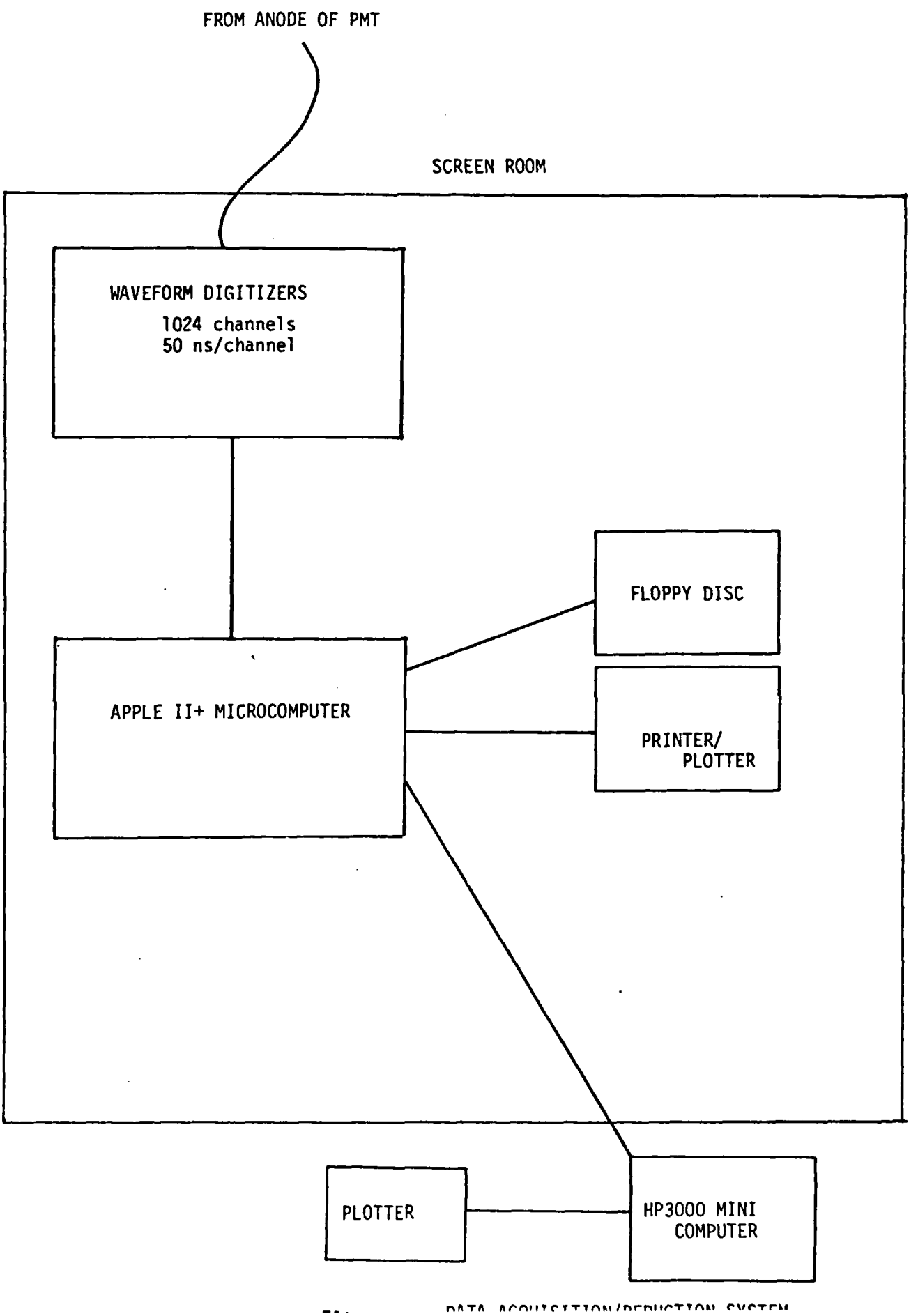

DATA ACQUISITION/REDUCTION SYSTEM

photomultiplier (RCA 7265). Anode signals are routed to an EMI screen room that houses the electronics for a CAMAC computer-controlled data acquisition/reduction system. Two wave-form digitizers (LeCroy, Model 2256A) allow observation of the transient PMT signal sampling with integration periods as fast as 50ns. Future multiplexing of the digitizers will increase time resolution to 25ns/sampling period. In addition, a variable pre-triggering capability allows accurate baseline records. An on-line microcomputer (Apple II PLUS) controls all digitizer functions as well as data accumulation, handling and storage (floppy disk). An off-line minicomputer (HP 3000) and digital plotter are currently utilized to display processed data. Oscilloscope display of electron-beam voltage and current waveforms allows rejection of data due to e-beam malfunction (e.g. pre-fire, pre-divert, excessive cathode flaring, synchronization problems, etc.). Due to the exceptional reproducibility of e-beam characteristics, to date, only prefire has caused data rejection.

IV. Recent Experimental Results

Large He(2^3S) metastable densities are necessary for efficient operation of the laser amplifier based on radiative collisions described in Section II. Preliminary results for a pure He plasma at 700Torr indicates, based on 3889Å radiation absorption (He($2^3S \rightarrow 3^3P$), that the peak absorption is 65 %(see Figure 15). Estimates of the metastable density based on this measurement indicate peak densities (i.e. at the beginning of the afterglow) of between 10^{13} and $10^{14}/cm^3$ which agrees well with previous theoretical predictions.[9] Absorption measurements for the He-N_2 plasma are not complete at this time but indicate that introduction of between .01% and 1% N_2 lowers the metastable density by roughly one and two orders of magnitude, respectively, in both the active discharge and the afterglow.

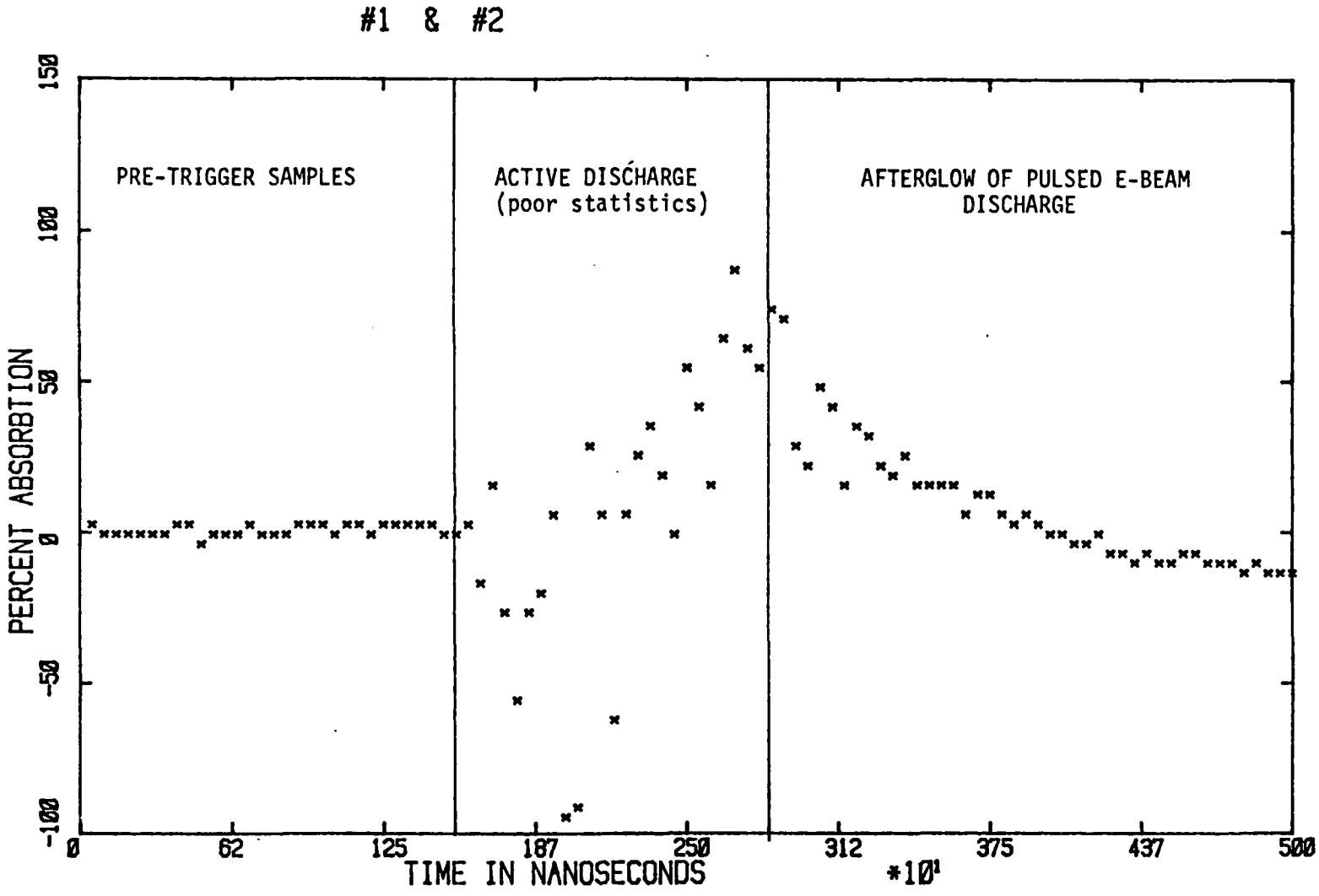

Figure 15. Per cent absorption at 3889Å.

Upon the addition of N_2 the optical emission due to the normal Penning transfer to N_2 becomes an indicator of $He(2^3S)$ density and, in the afterglow, a measure of the $He(2^3S)$ destruction rate.[10] Figure 16 shows a typical emission profile we measure for the $N_2^+(B\rightarrow X)$ at 3914Å. This permits experimental verification of the predicted stimulated emission due to radiative collisions presented in Section II. If, in the afterglow, a high pwoer density (10kW/cm^2 or higher) dye laser pulse at 3538Å is directed through the plasma then, within the volume of the plasma interacting with the laser pulse, radiative collisions should give stimulated emission at that wavelength. Simultaneous observation of 3914Å radiation should show a decrease in intensity due to the increase in the destruction rate of $He(2^3S)$ metastables that feed both the 3914Å spontaneous emission and the 3538Å stimulated emission from the radiative collision. It should also be noted that absence of $He(2^1S)$ metastables and helium ions during the afterglow[10] precludes the possibility that the energy transfer to N_2 and subsequent optical emission are due to any species other than $He(2^3S)$ metastables. Spontaneous emission from reaction (7) has also been measured using the system described in Section III (see Figure 17) as well as in a flowing afterglow experiment.

Emission of light at 3532Å and 3538Å has been detected in flowing afterglow experiments. Figure 18 depicts the flowing afterglow apparatus in which a high speed Roots vacuum pump is used to maintain a high speed, low pressure (~10m/s, 1 Torr) gas flow. In this experiment, helium is flowed through an electrical discharge and into a sample tube. Along the flow, distance from the discharge is directly proportional to the time into the afterglow. Nitrogen is introduced into the helium flow five centimeters (about five milliseconds) after the discharge. The nitrogen reacts with the long-lived helium excited states which survive the five millisecond flow. The reaction is monitored by optical spectroscopy on the light emitted by the short-lived nitrogen excited states produced in the reaction.

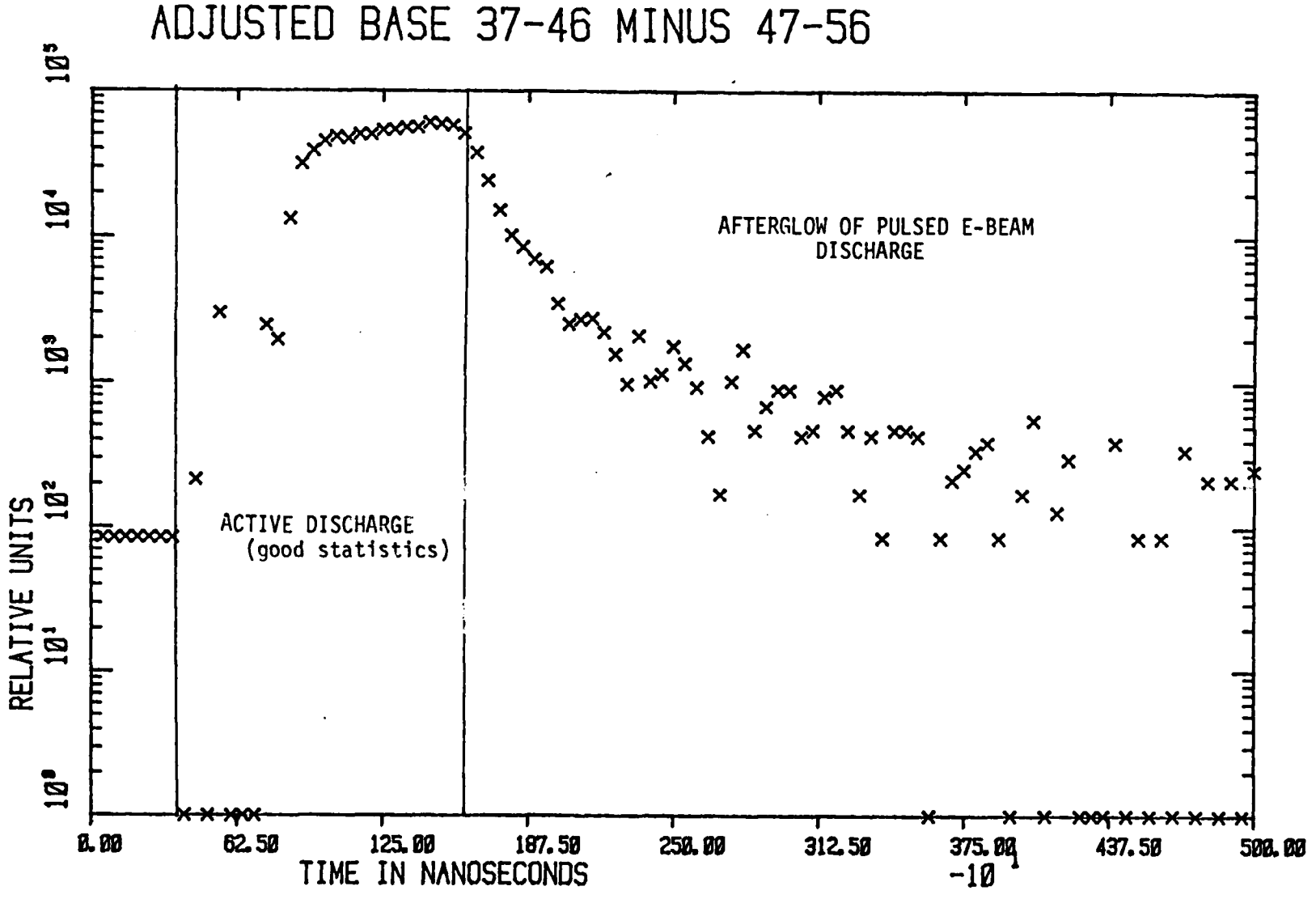

Figure 16. Emission at 3914Å showing stationary afterglow.

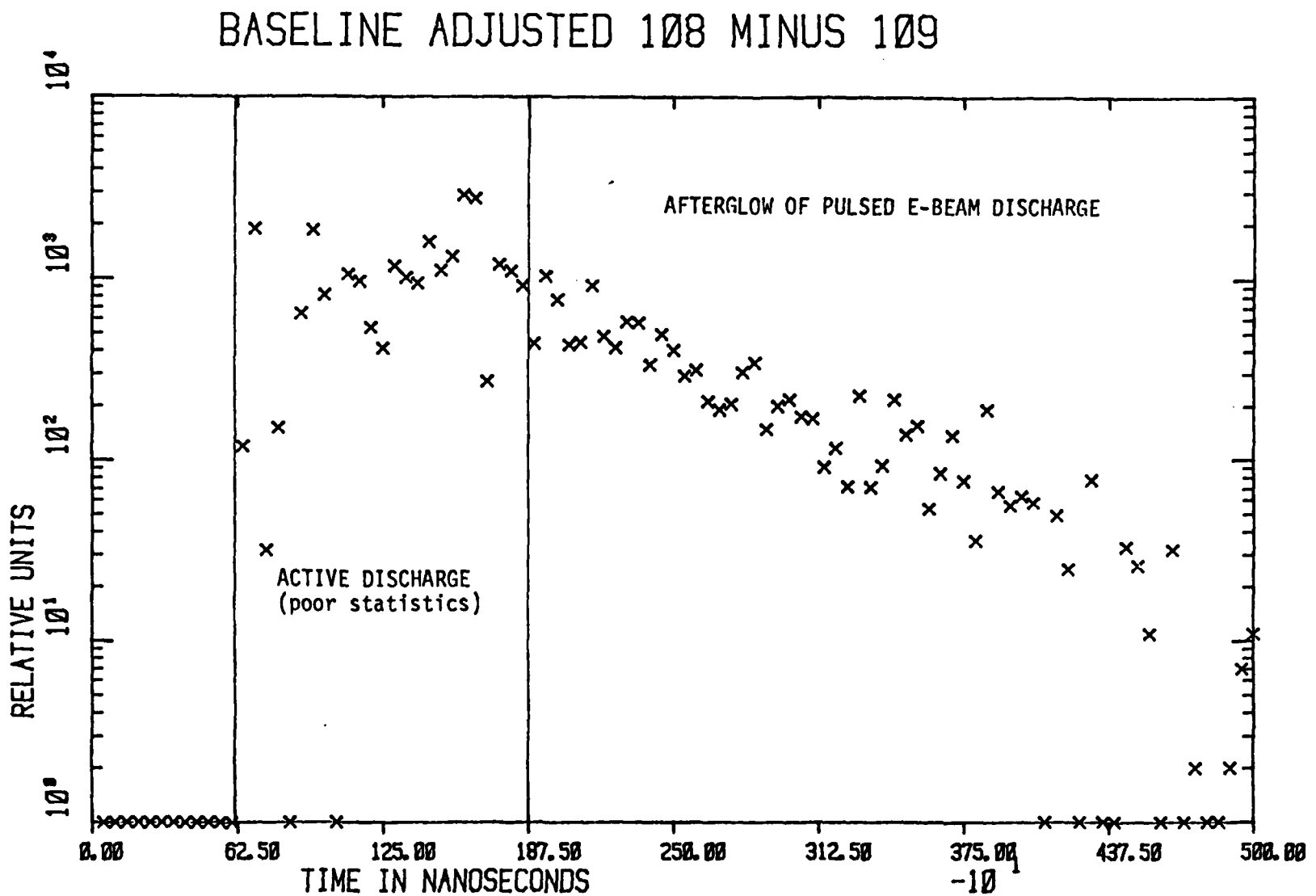

Figure 17. Emission at 3538Å showing stattionary afterglow.

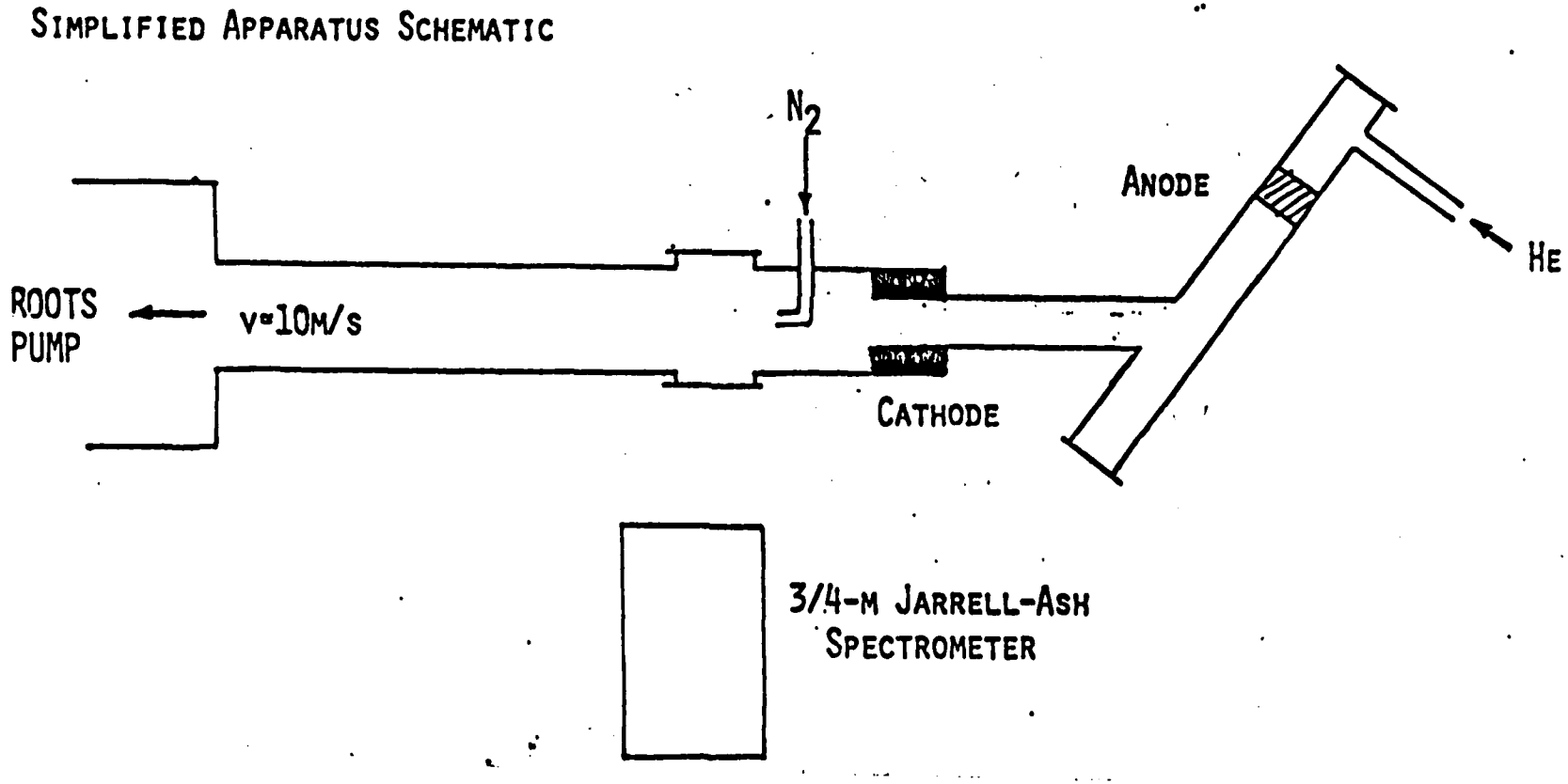

Figure 18. Simplified schematic of flowing afterglow apparatus.

The helium is excited in a low current (~10mA) discharge. In afterglow discharges of this type, $He(2^3S)$ is the dominant excited species. The other long-lived excited states are He^+ and $He(2^1S)$. Helium ions (and electrons) which are produced in small concentrations in the discharge are lost in the afterglow through ambipolar diffusion to the walls. The $He(2^1S)$ is produced in large quantities in the discharge but is lost quickly in the afterglow due to superelastic collisions with free electrons. In experiments of this kind, $He(2^1S)$ concentration is typically one or two percent of the $He(2^3S)$ concentration and the He^+ concentration is negligible. Hence the only significant reaction is $He\ (2^3S) + N_2 \rightarrow$ products.

Figure 19 shows two spectra of the nitrogen product emission. The second spectra is taken at ten times the sensitivity. From the spectrum one can determine that the nitrogen emission at 3582Å is 5% of the emission level at 3914Å. This is a lower limit since both the spectrometer and photomultiplier sensitivities peak at larger wavelengths. Figure 20 depicts the emission spectrum between 3500Å and 3600Å. Emission at 3532Å and 3538Å corresponds to the $N_2^*(B,5) \rightarrow N_2^*(X,4)$ and $N_2^*(B,4) \rightarrow N_2^*(X,3)$ transitions, respectively. Depending on how one interprets background, these both have one quarter to one half the intensity of 3582Å, or around 2% of the intensity of 3914Å.

A verification of the ratio of the intensity of 3538Å radiation to that of 3914Å radiation from the flowing afterglow experiment can be obtained from the electron-beam results shown in Figures 16 and 17. Since the 3914Å radiation plotted in Figure 16 and the 3538Å emission plotted in Figure 17 were taken under identical experimental conditions, the ratio of the intensities I_{3538}/I_{3914} can be found directly from the raw data. The ratio calculated in that way (1.9%) agrees very well with that found in the flowing afterglow experiment (2%). Figure 21 shows that the radiation at 3538Å seen in the electron beam results has a profile compatible with that of the flowing afterglow spectrum, Figure 20.

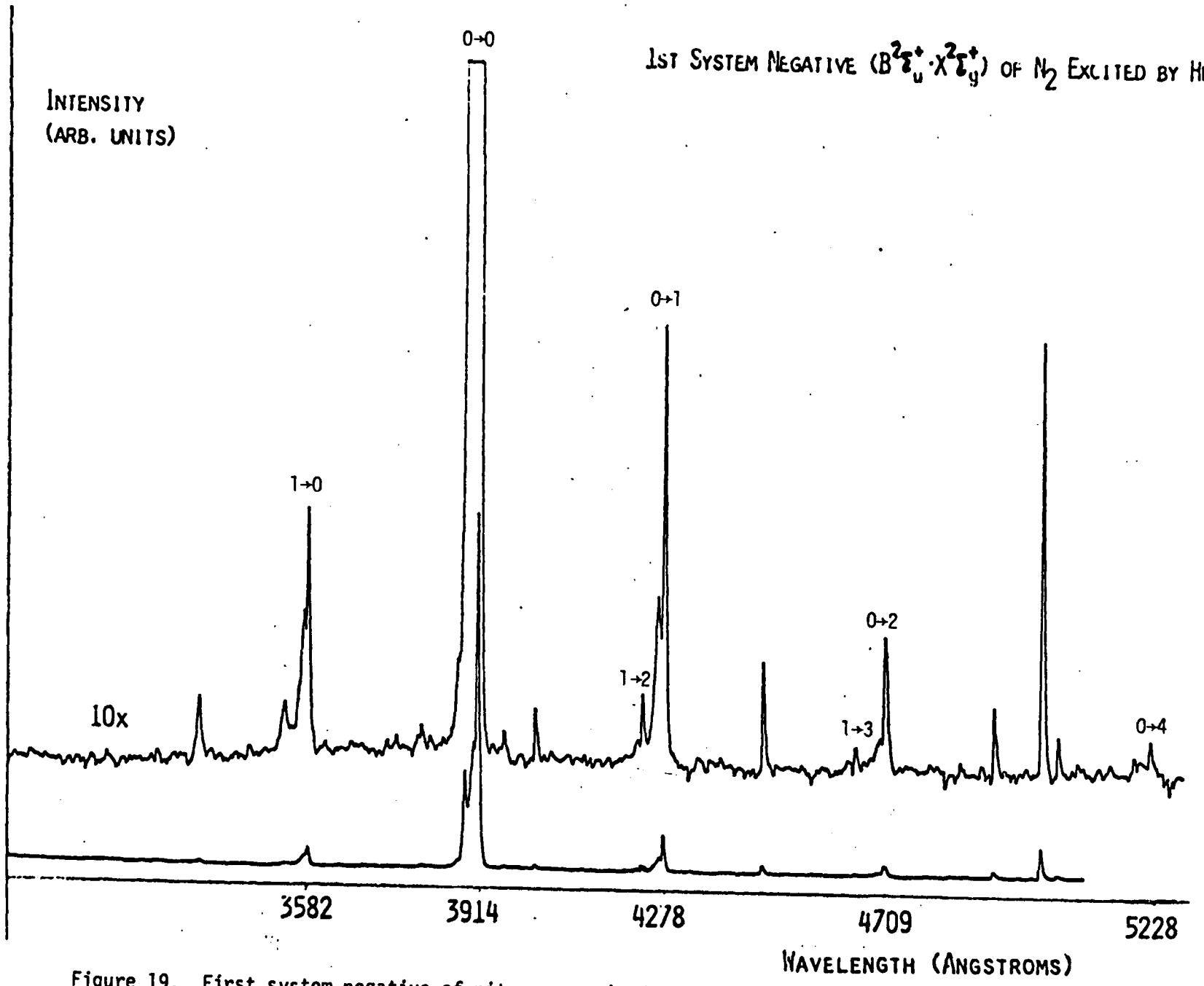

Figure 19. First system negative of nitrogen excited by the triplet helium metastable.

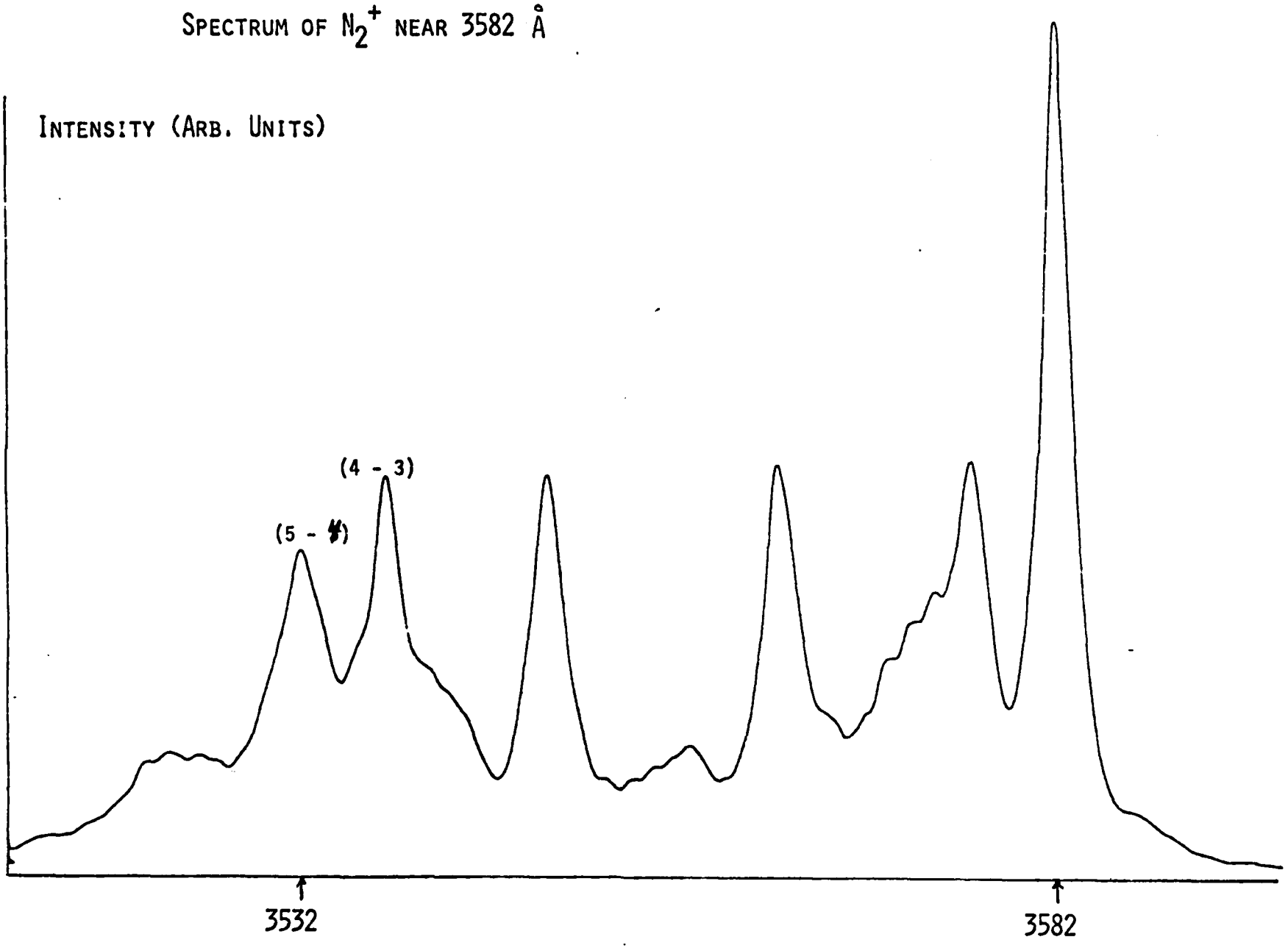

Figure 20. Nitrogen emission between 3500Å and 3600Å.

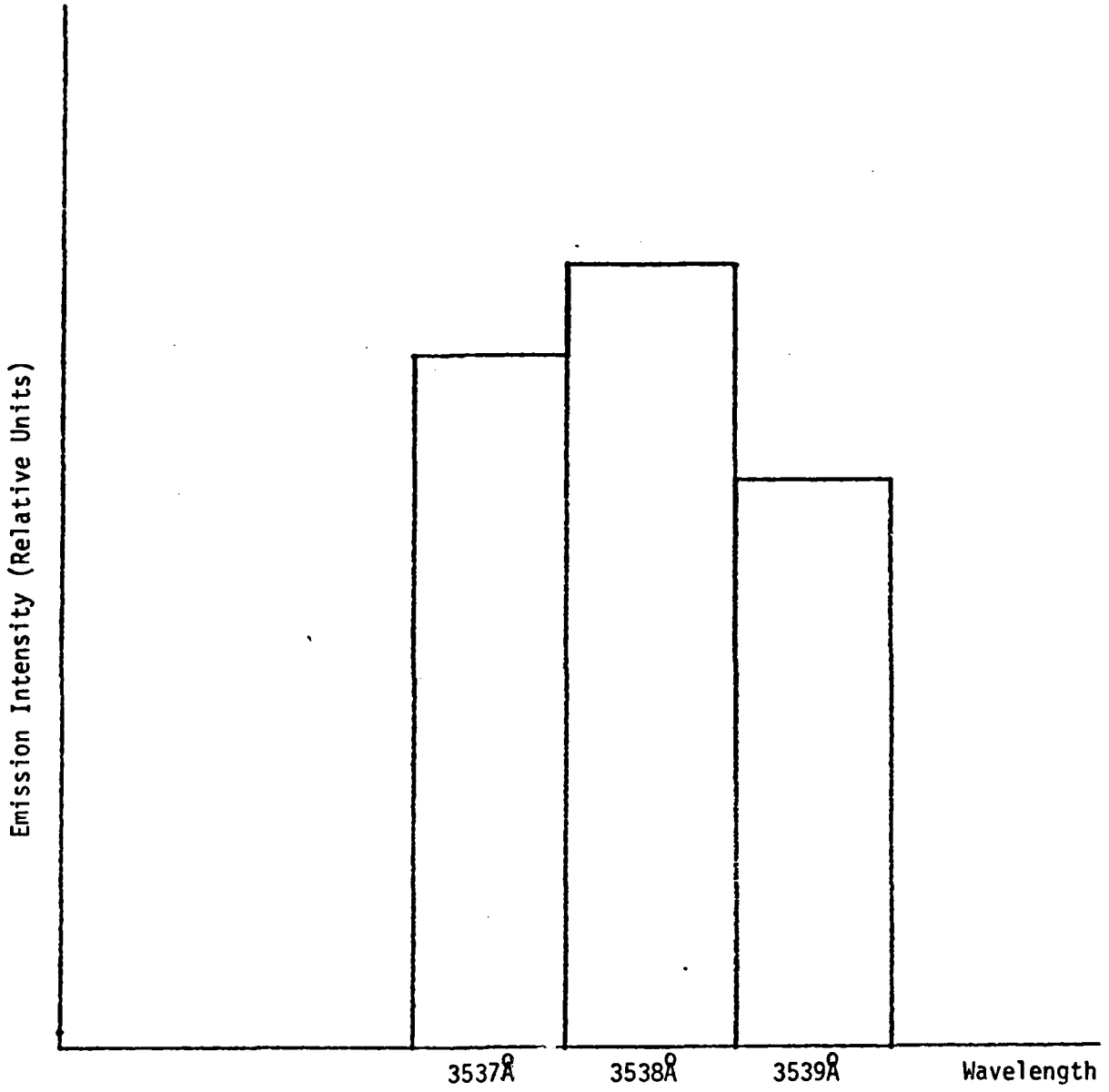

Figure 21. Profile of 3538Å emission 1μs into the afterglow (time resolution is 200ns). The statistical error in all cases is about 4%.

Following the analysis in Section II, the ratio I_{3538}/I_{3914} gives us an experimental verification of the calculated radiative collision cross-section. This can be seen as follows. The production of 3914 radiation can be expressed as

$$kI_{3914} = |I_{3914}| = \langle\sigma_p v\rangle [M][N_2], \tag{12}$$

where σ_p is the cross-section for the indicated Penning reaction scaled according to the branching ratio and all other symbols are as in Section 2, [M] represents the $He(2^3S)$metastable density and k is a detection system response coefficient. Similarly, for the 3538Å radiation intensity,

$$kI_{3538} = |I_{3538}| = A[M][N_2], \tag{13}$$

where A is the Einstein A coefficient. It should be noted here that, as in Section II, we are defining effective Einstein coefficients, i.e.,

$$A^{\text{Effective}}_{\text{Einstein}} = A[M], \text{ and} \tag{14}$$

$$B^{\text{Effective}}_{\text{Einstein}} = B[M]. \tag{15}$$

Taking the ratio of 13 to 12 gives

$$\frac{I_{3538}}{I_{3914}} = \frac{A}{\sigma_p v} \tag{16}$$

Recall that for radiative collisions (equations 4 and 6),

$$\langle\sigma_{RC} v\rangle = B\,\rho(\nu)\ , \tag{17}$$

where σ_{RC} is the radiative collision cross section.
The ratio[11] of the Einstein coefficients is

$$\frac{A^{\text{Effective}}_{\text{Einstein}}}{B^{\text{Effective}}_{\text{Einstein}}} = \frac{A}{B} = \frac{8\pi h\nu^3}{c^3} \tag{18}$$

From 16, 17 and 18, it is seen that

$$A = \frac{I_{3538}}{I_{3914}}\sigma_p v = \frac{8\pi h\nu^3}{c^3}\ \frac{\sigma_{RC} v}{\rho(\nu)} \tag{19}$$

where $\rho(\nu)$ is the energy density per unit frequency. If $\rho(\nu)$ is peaked at a particular frequency ν_0, then

$$\rho(\nu_0) = \rho_\nu g(\nu_0) = I_{\nu_0}/c\ \delta\nu_0 \tag{20}$$

where I_{ν_o} is the radiation intensity in W/m^2, $g(\nu_o)$ is the linewidth distribution and $\delta\nu_o$ is the linewidth[11]. From 19 and 20

$$\sigma_{RC} = \frac{I_{3538}}{I_{3914}} \frac{c^2}{8\pi h\nu^3} \sigma_P \frac{I_{\nu_o}}{\delta\nu_o} \tag{21}$$

or

$$\sigma_{RC} = \frac{I_{3538}}{I_{3914}} \frac{\lambda^3}{4hc} \sigma_P \frac{I_{\omega_o}}{\delta\omega_o} \tag{22}$$

Using the measured ratio of I_{3538}/I_{3914}, a linewidth of 2 cm^{-1} ($\delta\omega_o = 3.8 \times 10^{11}$ sec^{-1}) and $I_{\omega_o} = 10^3$ W/cm^2 gives

$$\sigma = 1.4 \times 10^{-17} \text{ cm}^2 \tag{23}$$

or

$$\sigma = 1.4 \times 10^{-20} \text{ cm}^4/\text{W} \ (I_{\omega_o}) \tag{24}$$

where, now, I_{ω_o} is in W/cm^2. This is shown on Figure 22 and the strong field results are inferred from theory. It is evident that the theory agrees well with this indirect measurement of the cross-section.

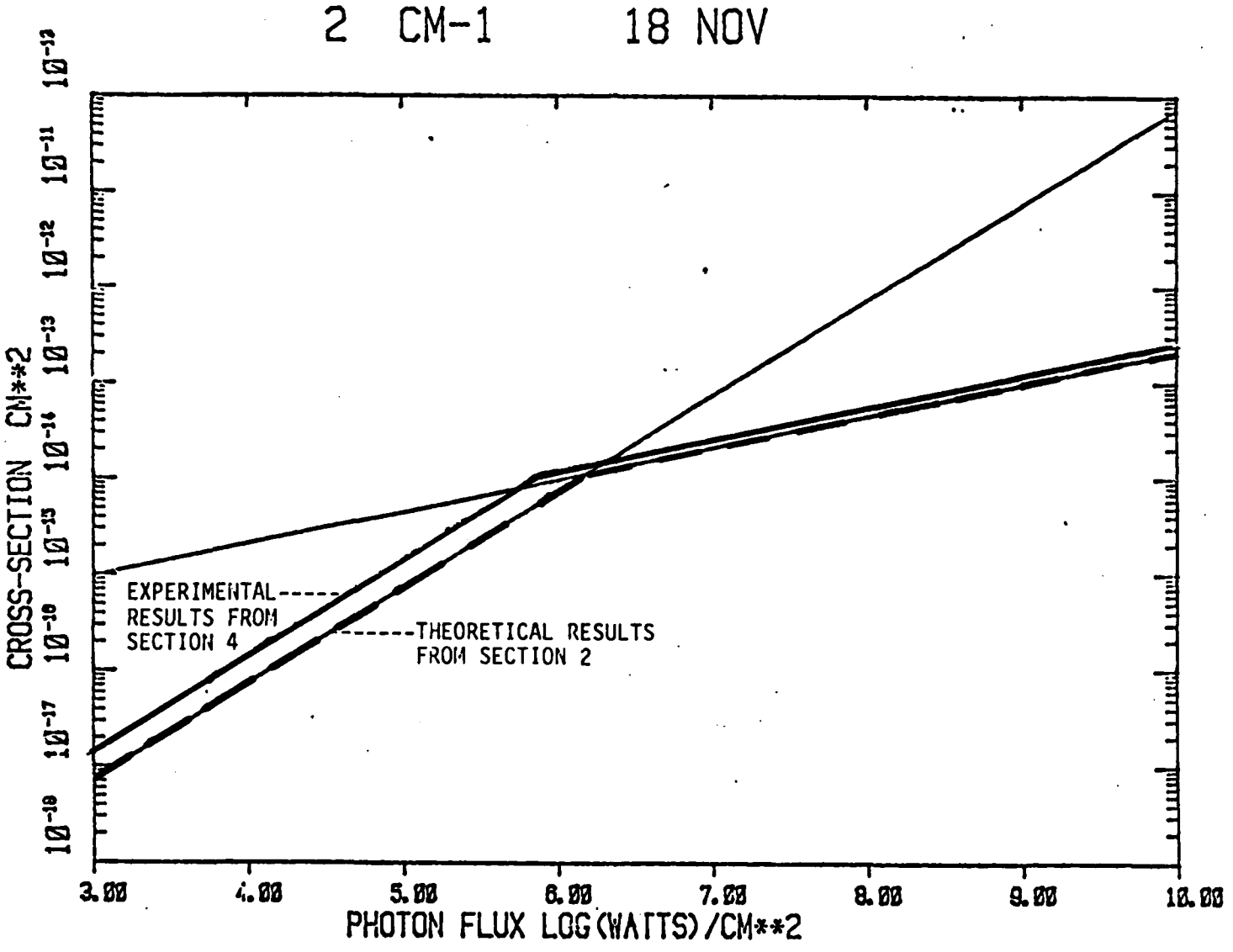

Figure 22. INFERRED EXPERIMENTAL AND THEORETICAL CROSS-SECTIONS AS A FUNCTION OF PHOTON FLUX FIELD.

V. Conclusions

In this report we have proposed a new method of stimulated emission from radiative-collisions, developed a theoretical model for the helium-nitrogen system in which a theoretical radiative-collisional cross section was calculated, and reported an indirect measurement of this cross section from observation of the spontaneous emission associated with reaction (7). These last measurements were done both in a low pressure flowing afterglow and in a high pressure electron-beam initiated static afterglow. The theoretical and measured values agree to within a factor of two. The prospects for the development of a high power/high energy laser amplifier by this new process are extremely attractive.

VI. Continuing Work

1) Efforts are being initiated to observe stimulated emission from radiative collisions in the He-N_2 system.

2) Preliminary plans are under investigation for the demonstration of a laser amplifier in collaboration with another laboratory.

3) Other systems are being explored in an effort to identify efficient laser or laser amplifiers. Particular attention is being given systems which may employ UF_6 in the lasing medium.

References

1) L.I. Gudzenko and S.I. Yakovlenko, "Radiative Collisions", Soviet Physics JETP, 35 (1972) 877.

2) L.W. Downes, S.D. Marcum, R.A. Tilton, and W.E. Wells, to be published.

3) S.E. Harris, J.F. Young, W.R. Green, R.W. Falcone, J. Lukasik, J.C. White, J.R. Willison, M.D. Wright and G.A. Zdasiuk, "Laser Induced Collisional and Radiative Energy Transfer", Proceedings of Laser Spectroscopy IV, June 1979.

W. R. Green, M.D. Wright, J. Lukasik, J.F. Young and S.E. Harris, "Observati of a Laser-induced Dipole-quadrupole Collision", Optics Letters, 4 (1979) 26

4) S.E. Harris, "Proposal for a 207 Å Laser in Lithium", Optics Letters, 5 (1980).

J.C. White, "Switched Photodissociation: A Proposal for the Inversion of Atomic and Molecular Species", Optics Letters, 5 (1980) 199.

5) J.-L. Delcroix, C.M. Ferreira and A. Ricard, "Metastable Atoms and Molecules in Ionized Gases" in Principles of Laser Plasmas edited by G. Bekefi (John Wiley and Sons, New York, 1976).

6) R.W. Nicholls, "Franck-Condon Factors to High Vibrational Quantum Numbers I: N_2 and N_2^+ ", Journal of Research of the National Bureau of Standards, 65A (1961) 451.

7) C. Duzy and R.S. Berry, "Autoionization of N_2", Journal of Chemical Physics, 64 (1976) 2431.

8) W.C. Richardson and D.W. Setser, J. Chem. Phys. 58 (1972) 1809.

9) B.D. DePaola, S.D. Marcum, H.K. Wrench, B.L. Whitten and W.E. Wells, "Estimations of electron densities and temperatures in ^{3}He dominated plasmas" in First International Symposium on Nuclear Induced Plasmas and Nuclear Pumped Lasers (Les Editions de Physique, May 23-25, 1978) 133.

10) T. Ueno, A. Yokoyama, S. Takao, and Y. Hatano, "De-excitation Rate Constants of He(2^3S) by Atoms and Molecules as Studied by the Pulse Radiolysis Method", Chemical Physics 45 (1980) 261-271.

11) A. Yariv, Quantum Electronics (John Wiley and Sons, New York, 1967).

the short-lived nitrogen excited states produced in the reaction.

END

DATE FILMED

9 — 83

DTIC